Maximal tripartite entanglement between singlet-triplet qubits in quantum dots

Tuukka Hiltunen and Ari Harju
COMP Centre of Excellence, Department of Applied Physics, Aalto University, Helsinki, Finland
(Received 27 September 2013; revised manuscript received 4 March 2014; published 28 March 2014)

We propose an efficient three-qubit gate of singlet-triplet states in quantum dots based on capacitative coupling. This scheme can be used to generate the maximally entangled Greenberger-Horne-Zeilinger state with one simple gate operation. Our simulations using a realistic microscopic model combined with our detailed analysis for the gate operation can be used to extract the actual experimental pulse sequence needed to realize this.

DOI: 10.1103/PhysRevB.89.115322 PACS number(s): 73.63.Kv, 03.67.−a, 73.21.La

I. INTRODUCTION

Entanglement is an essential resource in quantum-information technology. It is exploited in, for example, quantum teleportation, and entangled states are at the heart of all quantum computation [1]. Entanglement is, however, fragile to the environment, and it cannot generally be increased with local operations if the involved parties are not in direct contact [1,2]. The development of efficient methods for generating highly entangled states is thus an important task.

In contrast to the bipartite case, where all maximally entangled states are equivalent up to local operations [2], genuine tripartite entanglement exhibits two different classes, the W states [1,2] and the Greenberger-Horne-Zeilinger (GHZ) states [3]. The GHZ states, represented by $|\mathrm{GHZ}^{\pm}\rangle = (|000\rangle \pm |111\rangle)/\sqrt{2}$, are especially interesting, as they exhibit the strongest possible entanglement and correlations in a tripartite system [2]. In quantum information, they have applications in, for example, quantum teleportation [4] and dense coding [5]. The tripartite GHZ state belongs in the class of cluster states [6–8], highly entangled many-qubit states that are exploited in measurement-based quantum computing [9,10]. Previously, the GHZ states have been demonstrated in, for example, superconducting qubits [11,12] and theoretically proposed in, for example, single-spin qubit systems [13,14].

A promising realization for a quantum bit [15,16] is the two-electron spin eigenstates in quantum dots (QD) [17–19]. The universal set of quantum gates [20] for two spin singlet-triplet qubits has been demonstrated experimentally [21–23]. In this architecture, the interqubit interactions can be implemented using capacitative coupling that exploits the differences between the charge configurations of the singlet and triplet states to generate entanglement between the qubits [24,25]. The scheme, a two-qubit capacitatively coupling CPHASE gate, has been realized experimentally quite recently [23,26].

In this paper, we propose a generalization of the CPHASE gate, a capacitative three-qubit gate that creates tripartite entanglement between singlet-triplet qubits. The qubits are placed in the corners of a triangle. As they are evolved under exchange interaction, generated by electronically detuning the qubits, they start to entangle and disentangle. We quantify the classes of entanglement generated in the gate and show that a GHZ state can be obtained by the gate operation.

Our method provides an efficient way to generate high-tripartite entanglement, as the gate operation does not include multiple steps, but just detuning the three qubits to the desired values of the exchange interaction. Our analysis can be used to determine the pulse sequences to be used in such a gate for the creation of long-lasting GHZ states, paving the way towards an experimental realization of these maximally entangled states and three-qubit interactions in the singlet-triplet qubit architecture.

The paper is organized as follows. In Sec. II, the model and methods used in this study are discussed. The generation of GHZ states via capacitative coupling of three qubits is simluated in Sec. III. An effective model for the three-qubit gate operation is derived in Sec. IV and the creation of long lasting GHZ states is discussed. In Sec. V, the effects of asymmetry on the scheme are analyzed.

II. MODEL AND METHODS

A system consisting of N_q singlet-triplet qubits ($N = 2N_q$ electrons and QDs) is modeled using an extended Hubbard model Hamiltonian,

$$H = \sum_{i=1}^{2N} E_i a_i^\dagger a_i - \sum_{i,j=1}^{2N} t_{ij} a_i^\dagger a_j + \sum_{i,j,k,l=1}^{2N} v_{ijkl} a_i^\dagger a_j^\dagger a_l a_k, \quad (1)$$

where E_i are the on-site energies at each QD, t_{ij} are the tunneling matrix elements between dots, and v_{ijkl} are the Coulomb-interaction matrix elements. Here the indices i, j, k, and l refer to both the spin and spatial degrees of freedom. $\{a_i^\dagger\}_{i\leqslant N}$ are the creation operators for the $\sigma_i = -1/2$ electrons at the sites from 1 to N, and $\{a_i^\dagger\}_{i>N}$ are those for the $\sigma_i = +1/2$ electrons. Spin is conserved in the tunneling, i.e., $t_{ij} = \delta_{\sigma_i\sigma_j} t_{ij}$.

In Eq. (1), the Coulomb interaction is long range, $v_{ijkl} = \langle i|\langle j|\frac{C}{|\mathbf{r}_1-\mathbf{r}_2|}|l\rangle|k\rangle$. With $|i\rangle$ being δ functions in the Hubbard model, the v_{ijkl} elements can be written as

$$v_{ijkl} = \delta_{ik}\delta_{jl}\left[(1-\delta_{ij})\frac{C}{|\mathbf{r}_i - \mathbf{r}_j| - d} + \delta_{ij}U\right]. \quad (2)$$

Here, $C = e^2/4\pi\epsilon_r\epsilon_0$ is the Coulomb -strength, $\mathbf{r}_i$ and $\mathbf{r}_j$ are the locations of the dots i and j. U is the on-site interaction between two electrons in the same QD and $d > 0$ is an extra constant conveying the fact that in truth the wave functions have finite widths.

In the capacitative coupling, the tunneling between two S-T_0 qubits is usually negligible [23–26]. Hence, in our model,

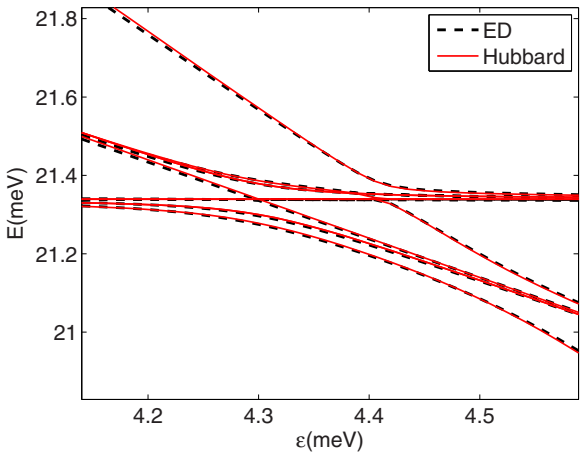

FIG. 1. (Color online) The lowest energies of a two-qubit system as a function of the detunings $\epsilon_1 = \epsilon_2 = \epsilon$. The thick black dashed line shows the ED energies, and the solid red line shows the Hubbard energies with the parameters $t_{ij} = 27.8$ μeV, $U = 3.472$ meV, and $d = 0.43$ nm.

the tunneling elements t_{ij} are nonzero only between the two dots inside the qubits. Consequently, we can include only the terms with exactly two electrons in each qubit in the Hubbard calculations (this is found to have no effect on the results shown in this paper and it makes the computations considerably faster). The Hamiltonian of Eq. (1) is diagonalized in the $S_z = 0$ subspace (i.e., the number of both up and down electrons is N_q) to obtain the eigenstates of the system.

The parameters t_{ij}, U, and d can be fitted to exact diagonalization (ED) data [27] in order to produce realistic results. We compare the Hubbard results to a reference system of two capacitatively coupled S-T_0 qubits (four QDs) modeled as parabolic potential wells. The parabolic dot minima are located at the x axis. The dot distances in the qubits are 80 nm, and the interqubit distance is 120 nm. The parabolic confinement strength is $\hbar\omega_0 = 4$ meV. The GaAs value of $\epsilon_r \approx 12.7$ is used for the permittivity. The many-body basis of Slater determinants is created using the single-particle eigenstates of the system which are computed using the multicenter Gaussian method [28]. The many-body Hamiltonian is diagonalized using the Lanczos method. See Ref. [27] for more details on the ED calculation.

A good fit is obtained with the values $t_{ij} = 27.8$ μeV, $U = 3.472$ meV, and $d = 0.43$ nm. The lowest energies (including the relevant two-qubit states $|SS\rangle$, $|ST_0\rangle$, $|T_0S\rangle$, and $|T_0T_0\rangle$) can be seen in Fig. 1 as a function of the detunings ϵ_1 and ϵ_2. (ϵ_n is the difference of the on-site energies E between the two dots of the qubit n.) Here, $\epsilon_1 = \epsilon_2 = \epsilon$. The energies computed with the two methods coincide almost exactly. The obtained parameters were also tested in asymmetric detuning cases, $\epsilon_1 \neq \epsilon_2$, and the fit was equally good there. As the strength of the capacitative interaction is determined by the energy differences of the two-qubit basis states, our Hubbard model should now describe the qubit-qubit interactions realistically (at least with the intra- and interqubit dot distances used).

III. GHZ STATE GENERATION

In the (symmetric) three-qubit gate, the qubits are placed at the corners of an equilateral triangle (both the inner and outer dots of the qubits form an equilateral triangle). The distance of the qubits (i.e., the distance of the inner dots) is 120 nm, and the intraqubit dot distance is 80 nm, as in the two-qubit case discussed in the previous section. The symmetric three-qubit geometry is illustrated in Fig. 2. The parameters of the Hubbard model correspond to the two-qubit system with $\hbar\omega_0 = 4$ meV confinement, 80 nm intraqubit dot distance, and 120 nm qubit-qubit distance (i.e., the values are the same as those in Fig. 1). The results shown in this paper all correspond to these Hubbard-parameter values. The same scheme was tested also with other intra- and interqubit distances (the parameters were again fitted to corresponding two-qubit gauss-ED data), and the results were qualitatively similar to the ones shown in this section.

The three-tangle, τ_{123}, measures the tripartite-entanglement in a three-qubit system [2,29]. Writing an arbitrary state $|\psi\rangle$ of the three qubits as $|\psi\rangle = \sum_{i,j,k=0}^{1} a_{ijk}|ijk\rangle$, with $|ijk\rangle = |i\rangle_1 \otimes |j\rangle_2 \otimes |k\rangle_3$, the three-tangle (for pure states) is given as

$$\tau_{123} = 2 \left| \sum a_{ijk} a_{i'j'm} a_{npk'} a_{n'p'm'} \times \eta_{ii'} \eta_{jj'} \eta_{kk'} \eta_{mm'} \eta_{nn'} \eta_{pp'} \right|, \quad (3)$$

where the sum goes from 0 to 1 for all indices, and $\eta_{01} = 1$, $\eta_{10} = -1$, and $\eta_{ii} = 0$. The value of τ_{123} is between 0 and 1, and it is maximal for the GHZ states. Conversely, the W class states have zero tangle. The entanglement in a subsystem of two qubits can be measured by pairwise concurrences. The pairwise concurrence C_{12} of qubits 1 and 2 can be computed from the reduced density matrix of the pair (see, e.g., Ref. [29] for the details). The W states maximize all three pairwise concurrences, so that $C_{12}^2 + C_{13}^2 + C_{23}^2 = 4/3$. In the GHZ states, the pairwise concurrences are zero [29].

We evolve the qubits under exchange (the detunings ϵ_i are held constant), so that the S and T_0 states have differing

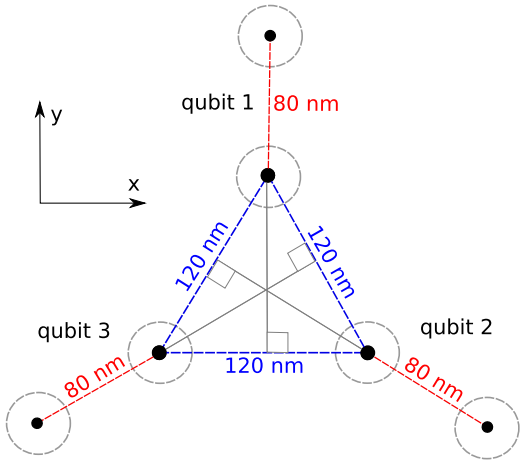

FIG. 2. (Color online) The geometry of the three-qubit system. The qubits are placed symmetrically at the corners of an equilateral triangle (both the inner and outer dots of the qubits form an equilateral triangle). The distance of the qubits (i.e., the distance of the inner dots) is 120 nm, and the intraqubit dot distance is 80 nm.

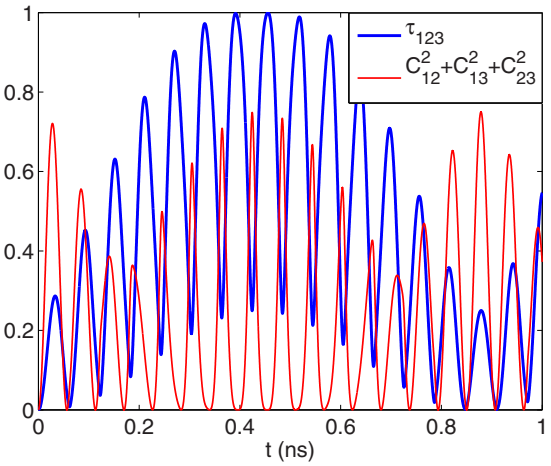

FIG. 3. (Color online) The evolution of the concurrences and the three-tangle with the detunings $\epsilon_1 = \epsilon_2 = \epsilon_3 = \epsilon = 3.9$ meV. The thick blue line shows the three-tangle and the solid red line shows the squared sum of the pairwise concurrences. At $t = 0$, all qubits are initiated in the xy plane of the Bloch sphere. The qubits are then allowed to evolve, and the concurrences and the three-tangle are computed at each time step.

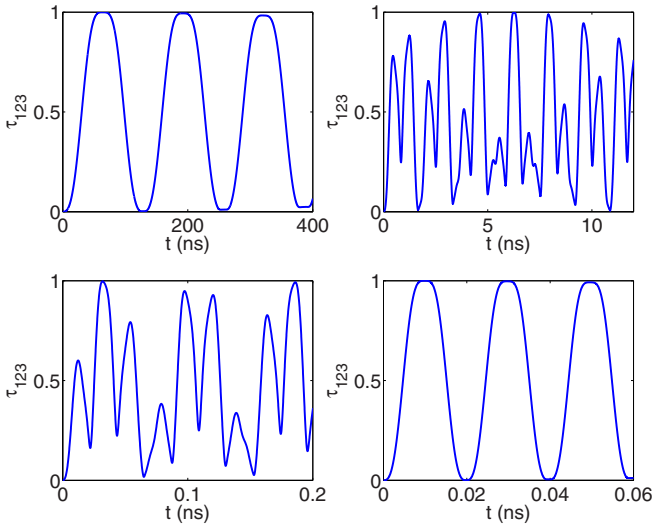

FIG. 4. (Color online) The evolution of the three-tangle with different detunings $\epsilon_1 = \epsilon_2 = \epsilon_3 = \epsilon$. At $t = 0$, all qubits are initiated in the xy-plane of the Bloch sphere. The qubits are then allowed to evolve, and the concurrences and the three-tangle are computed at each time step. Upper left plot corresponds to $\epsilon = 3.5$ meV, upper right to $\epsilon = 3.775$ meV, lower left to $\epsilon = 4.1$ meV, and lower right to $\epsilon = 4.5$ meV.

charge configurations. The time evolution of the full six-electron wave function $|\Psi\rangle$ is computed as $|\Psi(t + \Delta t)\rangle = \exp[-i\Delta t H(t)/\hbar]|\Psi(t)\rangle$, where $H(t)$ is the Hamiltonian (1) at time t. We project the wave function $|\Psi\rangle$ onto the three-qubit basis $\{|ijk\rangle\}_{i,j,k=0,1}$, and compute the three-tangle τ_{123} and the pairwise concurrences at each time step to study the entanglement properties of the system. Here, we write the singlet state S as 0 and the triplet state T_0 as 1.

Figure 3 shows the evolution of the concurrences in the case with the detunings held at $\epsilon_1 = \epsilon_2 = \epsilon_3 = \epsilon = 3.9$ meV (the further away dots are detuned to low potential). The system is initiated in a product state $|\Psi\rangle = |\psi\rangle_1 \otimes |\psi\rangle_2 \otimes |\psi\rangle_3$, with $|\psi\rangle_i = \frac{1}{\sqrt{2}}(|0\rangle + e^{i\phi_i}|1\rangle)$, with random phases ϕ_i. Both the pairwise concurrences and the three-tangle start to oscillate as the qubits are evolved. Both oscillations follow a similar modulated form, with fast carrier wavelike oscillations.

At around $t = 0.46$ ns, τ_{123} assumes the value of 1 (the exact numerical maximum being $\tau_{123} = 0.999\,998\,7$ in this simulation). At the same time, the pairwise concurrences are zero. These are both characteristics of GHZ states. Indeed, the state is found to be a GHZ state, $|\overline{\mathrm{GHZ}}\rangle$, that can be obtained from the more "typical" GHZ states $|\mathrm{GHZ}^\alpha\rangle = \frac{1}{\sqrt{2}}(|000\rangle + e^{i\alpha}|111\rangle)$ by single-qubit rotations. Generally, these one-qubit operations are given by rotating all three qubits the angle of $\pi/2$ around an axis $\hat{\mathbf{n}}(\varphi) = \cos(\varphi)\hat{\mathbf{x}} + \sin(\varphi)\hat{\mathbf{y}}$ that lies in the xy plane of the Bloch sphere. For example, the maximal tangle in Fig. 3 corresponds to rotating the qubits $\pi/4$ around the x axis ($\varphi = 0$) so that $|\overline{\mathrm{GHZ}}\rangle = e^{i\pi/4\cdot p(\mathbf{X}\otimes\mathbf{I}\otimes\mathbf{I}+\mathbf{I}\otimes\mathbf{X}\otimes\mathbf{I}+\mathbf{I}\otimes\mathbf{I}\otimes\mathbf{X})}|\mathrm{GHZ}^{\pi/2}\rangle$, where $\mathbf{I}$ is the identity, and $\mathbf{X}$ is the x-Pauli matrix.

The value of the detuning affects the operation of the three-qubit entangling procedure. Small detunings lead to small differences in the charge distributions of the qubit states and hence to slower operation. However, there are also qualitative differences between the concurrence oscillations with different detunings. The frequency of the carrier oscillations of τ_{123} varies in a quite complex manner compared to the modulating envelope's frequency as a function of the detuning ϵ. With small or very high values of the detunings ($\epsilon < 3.6$ meV or $\epsilon > 4.4$ meV), the modulation is very slow compared to the carrier oscillations. This is demonstrated in the upper-left and lower-right plots of Fig. 4. In these cases, it almost seems that there is no modulation at all, but just τ_{123} oscillating between 0 and 1. In contrast, with the intermediate detuning values (3.6 meV $\leqslant \epsilon \leqslant$ 4.4 meV), the oscillations can become quite complicated, with two or three modulating envelopes on top each other, as in the upper-right plot of Fig. 4.

IV. THREE-QUBIT GATE

When the detunings ϵ_n are held constant and there are no magnetic field gradients between the dots of the qubits, the three-qubit computational basis states are eigenstates of the Hamiltonian (1). This is due to the fact that, in the absence of magnetic field gradients and with constant detuning, the S and T_0 states are uncoupled in each of the three qubits [20,21] and that there is no tunneling between the qubits in our system (the qubit-qubit distances are long enough that there is no overlap between wave functions in different qubits). Projecting the Hubbard Hamiltonian onto the computational basis $\{|ijk\rangle\}_{i,j,k=1,2}$ thus results in a diagonal matrix (this was also confirmed numerically using the Hubbard model, and the off-diagonal terms were found to exactly zero up to double precision) with the energies of the basis states as its diagonal entries. The energies of the qubit basis states are governed by the exchange energy J and by the difference in the Coulomb repulsion between the singlet and triplet states in two neighboring qubits Δ. The exchange of, for example, qubit 1, J_1, is defined here as the energy

difference between $|001\rangle$ and $|000\rangle$, $J_1 = E_{001} - E_{000}$, and the Δ value of, for example, qubits 1 and 2 is denoted by $\Delta_{12} = E_{011} + E_{000} - E_{001} - E_{010}$.

Normalizing the energy of $|000\rangle$, E_{000}, to zero, one can write the energies of the computational basis states as $E_{001} = J_1$, $E_{010} = J_2$, $E_{100} = J_3$, $E_{011} = J_1 + J_2 + \Delta_{12}$, $E_{101} = J_1 + J_3 + \Delta_{13}$, and $E_{110} = J_2 + J_3 + \Delta_{23}$. Outside of the actual anticrossing area of the singlet charge states, it holds similarly that $E_{111} = J_1 + J_2 + J_3 + \Delta_{12} + \Delta_{13} + \Delta_{23}$. However, in the anticrossing area, when the singlets are in a superposition of the (1,1) and (0,2) charge states, their charge distributions depend also on the qubit basis state in question. In the doubly occupied triplet states, $|011\rangle$, $|101\rangle$, and $|110\rangle$, the repulsion in the inner dots of the triangle forces the singlets to localize into the outer dots with smaller detuning values compared to the other basis states. This pushing effect lowers the energies of the doubly occupied triplet states with respect to E_{111}, resulting in an additional contribution Δ_{123} to E_{111}, so that $E_{111} = J_1 + J_2 + J_3 + \Delta_{12} + \Delta_{13} + \Delta_{23} + \Delta_{123}$.

In the computational basis, the operation of the three-qubit gate with the detunings held constant can thus be described by a diagonal matrix with the aforementioned energies as its diagonal entries. Writing the state of the system as an eight-vector, $\mathbf{\Psi} = (\Psi_i)_{i=1}^{8}$, whose ith component corresponds to the qubit state that is the binary representation of $i - 1$, one can write the diagonal effective Hamiltonian as

$$\mathbf{H}_{\text{eff}} = -\frac{\hbar}{2}\left\{\sum_{n=1}^{3} J_n \mathbf{V}_n - \frac{1}{2}\sum_{n<m}\Delta_{nm}\mathbf{U}_{nm} + \frac{\Delta_{123}}{4}\left[(\mathbf{I}-\mathbf{Z})\otimes(\mathbf{I}-\mathbf{Z})\otimes(\mathbf{I}-\mathbf{Z})\right]\right\}. \quad (4)$$

Here, $\mathbf{V}_1 = \mathbf{I}\otimes\mathbf{I}\otimes\mathbf{Z}$, $\mathbf{V}_2 = \mathbf{I}\otimes\mathbf{Z}\otimes\mathbf{I}$, and so on. $\Delta_{nm}\mathbf{U}_{nm}$ describes the coupling of qubits n and m, with $\mathbf{U}_{12} = \mathbf{I}\otimes(\mathbf{I}-\mathbf{Z})\otimes(\mathbf{I}-\mathbf{Z})$ (and so on), where $\mathbf{Z}$ is the z-Pauli matrix. Note that the form of Eq. (4) is the same as in the two-qubit effective Hamiltonian in, for example, Refs. [23,30], apart from the third term with Δ_{123}. The third term describes an effective three-qubit interaction arising from the singlet charge distribution differences in the anticrossing area. Equation (4) is not restricted to S-T_0 qubits, it can in principle be used to describe the general case of three qubits coupled via CPHASE gates.

The evolution operator corresponding to the three-qubit gate operation with constant detunings is given by $\mathbf{U}(t) = \exp(-it\mathbf{H}_{\text{eff}}/\hbar)$. As $\mathbf{H}_{\text{eff}}$ is diagonal, the gate operation on an arbitrary state $|\Psi\rangle$ in the computational basis corresponds to multiplying each term $|ijk\rangle$ with a complex phase determined by the energy of the basis state. The gate can therefore be called a three-qubit version of the CPHASE gate.

In Eq. (4), the parameters J_n, Δ_{nm}, and Δ_{123} are functions of the detunings ϵ_1, ϵ_2, and ϵ_3. Figure 5 shows the detuning dependence of these parameters in the symmetric case, $\epsilon_1 = \epsilon_2 = \epsilon_3 = \epsilon$. As seen in the figure, the exchange J increases approximately exponentially before the anticrossing (located between $\epsilon = 3.6$ meV and $\epsilon = 4.4$ meV in this three-qubit system), after which it behaves linearly as expected. The pairwise coupling Δ also starts off exponentially in ϵ, saturating to a constant value when the singlets are fully in (0,2). The value stays approximately constant until decreasing to zero again at the triplet transition to $|T_0(0,2)\rangle$ that happens at much larger detuning [(0,2)-triplets cannot be simulated with our Hubbard model. In the two-qubit case, this transition happens at around $\epsilon = 6.5$ meV in our gauss-ED computations]. Δ_{123} has nonzero values only in the anticrossing area where the singlets are in a superposition of their charge states.

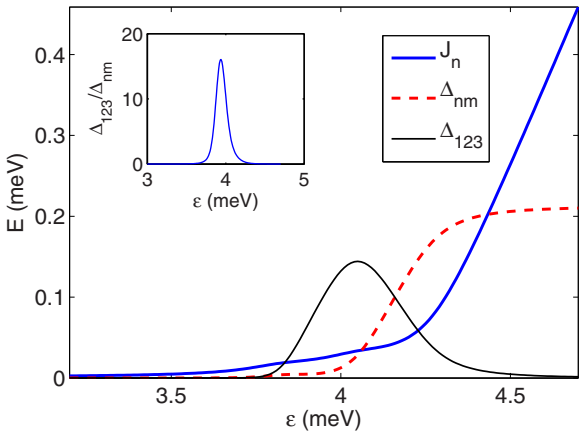

FIG. 5. (Color online) The detuning dependence of the parameters J_n, Δ_{nm}, and Δ_{123} of Eq. (4) in the symmetric case, $\epsilon_1 = \epsilon_2 = \epsilon_3 = \epsilon$ (the parameters are computed with the Hubbard model). The solid blue line shows the exchange J_n ($J_1 = J_2 = J_3$ due to symmetry), the dashed red line the two qubit coupling Δ_{nm} ($\Delta_{12} = \Delta_{13} = \Delta_{23}$ due to symmetry), and the thin black line the three-qubit coupling Δ_{123}. The inset shows the ratio Δ_{123}/Δ_{nm} as a function of the detuning ϵ.

In the general asymmetric cases, J_n increases as a function of ϵ_n similarly as in Fig. 5 and is approximately constant in the other two detunings (a small effect still remains resulting from the aforementioned push effect). The pairwise coupling Δ_{nm} is an increasing function of both ϵ_n and ϵ_m, again saturating to a maximum value when the singlets are in (0,2) in all of the computational basis states. The behavior of Δ_{123} is somewhat more complex. Δ_{123} is zero if any of the three qubits is below the anticrossing area and when they are all above it. If at least one of the qubits is in the anticrossing, and none of the qubits are below it, Δ_{123} assumes positive values.

The behavior of the tangle oscillations can be analyzed using the effective model, Eq. (4). As the system is symmetrical with respect to the three qubits, the parameters in Eq. (4) simplify to $J_1 = J_2 = J_3 = J$ and $\Delta_{12} = \Delta_{13} = \Delta_{23} = \Delta$. The qubits are initiated in the xy plane [for simplicity, now in the states $|\psi\rangle_i = \frac{1}{\sqrt{2}}(|0\rangle + |1\rangle)$, $i = 1,2,3$; a similar result applies for the general case]). In the notation of Eq. (4), the full six-body wave function is now written as $\mathbf{\Psi} = 1/\sqrt{8}\times[1,1,1,1,1,1,1,1]^T$. The qubits are evolved with constant detunings, (i.e., constant J, Δ, and Δ_{123}), so that each component of $\mathbf{\Psi}$ obtains a phase factor according to Eq. (4). Inserting the phases into Eq. (3) yields an analytic formula for the evolution of the three-tangle,

$$\tau_{123}(t) = \tfrac{1}{16}|e^{(2\Delta_{123}+4\Delta)it/\hbar} - 6e^{(\Delta_{123}+2\Delta)it/\hbar} + 4e^{\Delta it/\hbar} + 4e^{(\Delta_{123}+\Delta)it/\hbar} - 3|. \quad (5)$$

Equation (5) is indeed found to produce the same exact tangle oscillations observed in the simulations. The frequencies of the modulation and the carrier oscillations (e.g., in Fig. 3) are given by Δ and by $\Delta_{123}+\Delta$, respectively. However, the phase of the modulation varies, and in some cases, for example, with $\epsilon = 3.8$ meV, there is more than one modulation envelope on top of each other.

In the cases of low and very high detunings, Eq. (5) can be simplified. Outside of the anticrossing region, $\Delta_{123} \approx 0$ (relatively compared to Δ, see the inset in Fig. 5). With $\Delta_{123} = 0$, Eq. (5) simplifies to

$$\tau_{123}(t) = \tfrac{1}{4}\sqrt{[1-\cos(t\Delta/\hbar)]^3\,[5+3\cos(t\Delta/\hbar)]}. \quad (6)$$

Equation (6) oscillates between 0 and 1 with the frequency of $f = \Delta/2\hbar\pi$. We find that the corresponding oscillation frequency can also be determined by studying the pairwise concurrences, e.g., C_{12} in the case when only the qubits 1 and 2 are detuned, so that $\epsilon_1 = \epsilon_2 = \epsilon$, $\epsilon_3 = 0$. In this case, the pairwise concurrence is found to oscillate between 0 and 1 as $C_{12}(t) = \frac{1}{2}\sqrt{2-2\cos(2\pi f t)}$, with the same frequency f as in Eq. (6).

Equation (6) thus allows one to predict the moment when the $|\overline{\mathrm{GHZ}}\rangle$ state is obtained with the gate operation. It fits quite well with the slowly modulating tangle shown in Fig. 6, especially in the beginning of the oscillation. With longer gate operation, the tangle given by Eq. (6) starts to deviate more from the simulated one, as the modulation still exists (the further away the detunings are from the anticrossing area, the better $\Delta_{123} \approx 0$ holds).

In the anticrossing area, the singlet in, for example, $|110\rangle$ may be fully in the (0,2) state, while those of $|100\rangle$ are still in a superposition of $S(1,1)$ and $S(0,2)$ due to higher Coulomb repulsion between the inner dots in $|110\rangle$. In this case, $\Delta_{123} > 0$, and Eq. (6) no longer holds. Instead, τ_{123} evolves in a complex manner with carrier and envelope oscillations, as seen in Fig. 3.

Next, we discuss using the three-qubit gate to create a "long-lasting" GHZ state. The three-tangle keeps oscillating as long as the exchange interaction in the qubits is nonzero. In principle, turning the detunings off at the exact moment when τ_{123} has reached its maximum yields a stationary $|\overline{\mathrm{GHZ}}\rangle$ state (apart from decoherence effects [31–33] that are not currently included in our model). However, due to the effect of the charge state leakage [27], the detuning must be turned off gradually. However, if the detuning is decreased slowly enough to ensure an adiabatic passage from $S(1,1)$ to $S(0,2)$, the qubits keep interacting during the decrease, and the state is no longer the maximally entangled GHZ state.

With small detunings and slower gate operation (like in Fig. 6), the decrease times can be longer. In addition, smaller detunings can be turned off faster while still retaining adiabaticity. Also, the less chaotic oscillations with small detunings allow better predictability of the location of the τ_{123} maxima, via Eq. (6). In experiments, a longer gate-operation time means more decoherence. Hence, a compromise between fast operation and easy state preparation should be done in possible experimental realizations of this entangling scheme.

The procedure is demonstrated in Fig. 6 as the cyan (solid light) line. The qubits are again initiated in the xy plane and allowed to evolve under exchange. The detunings are $\epsilon = 3.5$ meV. When τ_{123} reaches its maximum, the detunings are decreased to zero linearly in 0.5 ns. When the detunings have reached zero, the system is allowed to evolve again. As seen in the figure, the three-tangle stays at its maximum after the detuning sweep.

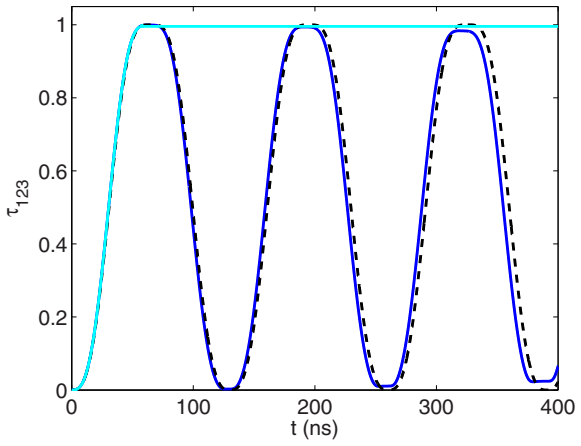

FIG. 6. (Color online) The evolution of the three-tangle with the detunings $\epsilon = 3.5$ meV. At $t = 0$, the qubits are initiated in the xy plane of the Bloch sphere. The qubits are then allowed to evolve, and the three-tangle is computed at each time step. The blue line (dark solid line) shows the three-tangle computed by projecting the wave function onto the qubit basis. The dashed black line shows the approximated tangle according to Eq. (6). The cyan line (light solid line) shows the long-lasting $|\overline{\mathrm{GHZ}}\rangle$ state obtained by switching off the detunings when τ_{123} reaches its maximum. Here, the detunings are decreased to zero in 0.5 ns, and the system is then allowed to evolve again.

V. EFFECTS OF ASYMMETRY

Last, we discuss the effect of asymmetry on the entanglement properties of the system [note that the asymmetrical

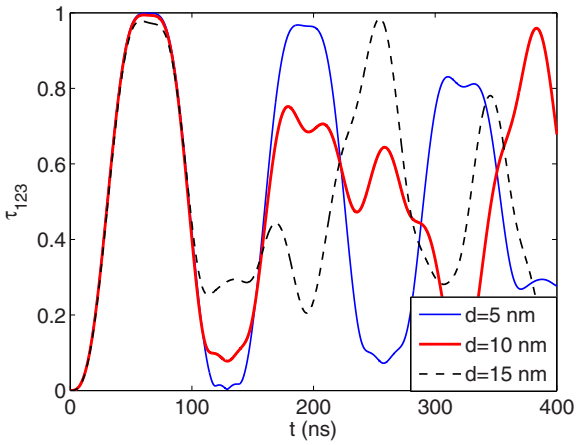

FIG. 7. (Color online) The effect of geometric asymmetry on the tangle oscillations. The qubit 1 in Fig. 2. is displaced from the symmetric configuration with a vector of length d, pointing in the positive x direction, so that $\tilde{\mathbf{r}}_{1,2} = \mathbf{r}_{1,2} + d\hat{\mathbf{e}}_x$. The tangle evolution is computed with the detunings held at $\epsilon = 3.5$ meV as in Fig. 6.

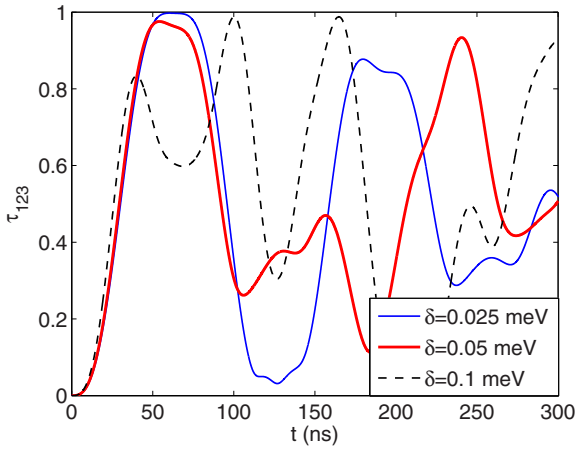

FIG. 8. (Color online) The effect of detuning asymmetry on the tangle oscillations. Detunings are set to $\epsilon_1 = \epsilon$, $\epsilon_2 = \epsilon + \delta$, and $\epsilon_3 = \epsilon - \delta$, with $\epsilon = 3.5$ meV, and the evolution of the three-tangle is computed.

cases are also described by the effective model of Eq. (4)]. The symmetry was broken by adding a small displacement vector $\mathbf{d}_i$ to the location of each dot, $\tilde{\mathbf{r}}_i = \mathbf{r}_i + \mathbf{d}_i$, or by using asymmetric detunings, $\epsilon_1 = \epsilon$, $\epsilon_2 = \epsilon + \delta_1$, and $\epsilon_3 = \epsilon + \delta_2$. Given the the vast number of degrees of freedom in these schemes to break the symmetry of the system, it is difficult to present a conclusive quantitative analysis on the effects of the asymmetry. We thus discuss some general qualitative features of the asymmetry properties and concentrate on a few selected special cases with more detail.

In Fig. 7, the geometrical symmetry of the system was broken by displacing qubit 1 with a vector of length d, pointing in the positive x direction (see Fig. 2), so that $\tilde{\mathbf{r}}_{1,2} = \mathbf{r}_{1,2} + d\hat{\mathbf{e}}_x$. The detunings were set to $\epsilon = 3.5$ meV (as in Fig. 6) and the tangle evolution was computed. As seen in the figure, the larger the displacement, the more chaotic the oscillations become. However, the form of the first tangle-peak at $t = 64$ ns stays very similar to the symmetric case in Fig. 6. The tangle values at the first peak in the $d = 5$ nm, $d = 10$ nm, and $d = 15$ nm cases are $\tau_{123} = 0.998$, $\tau_{123} = 0.996$, and $\tau_{123} = 0.978$, respectively. A quite general feature of the geometric asymmetry seems to be that the the oscillations often follow a form similar to that of the symmetric case at the beginning of the evolution (there are exceptions to this behavior, for example, with very large asymmetries). This results probably from the fact that the geometric asymmetry has little effect on the charge distributions of the qubit basis states.

The effect of the detuning asymmetry below the anticrossing region is demonstrated in Fig. 8. Asymmetry in only one of the detunings is not found to have a large effect on the tangle evolution even with asymmetries on the order of 0.1 meV. Hence, the detunings are set to $\epsilon_1 = \epsilon$, $\epsilon_2 = \epsilon + \delta$, and $\epsilon_3 = \epsilon - \delta$, with $\epsilon = 3.5$ meV, and the evolution of the three-tangle is computed. With small δ, at least the first peak is again preserved. However, as δ is increased above 0.05 meV, the oscillations take a form completely different from that of the symmetric case. Below the anticrossing area, the charge distributions and hence also the Coulomb repulsion between qubits are quite sensitive to the detunings.

Generally, the larger the asymmetry, the more chaotic the concurrence oscillations become, as the energies of the qubit states contain less symmetry ($|001\rangle$ and $|010\rangle$ are no longer degenerate, and so on). A maximal $\tau_{123} = 1$ GHZ state is still obtained at some point of the time evolution in all tested cases, even with very large dislocations or detuning differences (e.g., $|\mathbf{d}_i| = 15$ nm, $\delta_1 = -\delta_2 = 0.5$ meV). However, with large asymmetry the waveform of the concurrence oscillations no longer follows the modulated form of Eq. (6). Asymmetry in the geometry of the system results in the values of Δ_{nm} being different depending on the qubit pair in question, which then complicates the wave form of the concurrence oscillations given by the gate operation. Detuning asymmetry has a similar effect by causing differences in the charge distributions of the qubits. The system is thus susceptible to it below the anticrossing area when the rise of Δ_{nm} is exponential in ϵ. With large detunings [singlets fully in (0,2)], the detuning asymmetry has no effect on the concurrence oscillations.

VI. CONCLUSIONS

In conclusion, we have proposed an entangling three-qubit gate based on the capacitative coupling of singlet-triplet qubits. It provides a simple and efficient method for generating maximally entangled tripartite states in the singlet-triplet qubit architecture. We analyze the gate operation using an accurate microscopic model and find that a GHZ state can be generated. We derive an effective model for the gate operation and analytical formulas for the evolution of three-body entanglement. Using the formulas and our analysis, one can determine the detuning pulse sequences to be used for generating the GHZ states. We also show that, by turning off the detunings at the right phase of the oscillation, one can create a long-lasting GHZ state of maximal three-qubit entanglement.

ACKNOWLEDGMENTS

We thank Mikko Ervasti and Zheyong Fan for comments and suggestions. This research has been supported by the Academy of Finland through its Centres of Excellence Program (Project No. 251748).

[1] R. Horodecki, P. Horodecki, M. Horodecki, and K. Horodecki, Rev. Mod. Phys. **81**, 865 (2009).
[2] W. Dür, G. Vidal, and J. I. Cirac, Phys. Rev. A **62**, 062314 (2000).
[3] D. M. Greenberger, M. A. Horne, A. Shimony, and A. Zeilinger, Am. J. Phys. **58**, 1131 (1990).
[4] A. Karlsson and M. Bourennane, Phys. Rev. A **58**, 4394 (1998).
[5] J.-C. Hao, C.-F. Li, and G.-C. Guo, Phys. Rev. A **63**, 054301 (2001).
[6] H. J. Briegel and R. Raussendorf, Phys. Rev. Lett. **86**, 910 (2001).

[7] M. Borhani and D. Loss, Phys. Rev. A **71**, 034308 (2005).
[8] L. Amico, R. Fazio, A. Osterloh, and V. Vedral, Rev. Mod. Phys. **80**, 517 (2008).
[9] R. Raussendorf, D. E. Browne, and H. J. Briegel, Phys. Rev. A **68**, 022312 (2003).
[10] R. Raussendorf and H. J. Briegel, Phys. Rev. Lett. **86**, 5188 (2001).
[11] L. DiCarlo, M. D. Reed, L. Sun, B. R. Johnson, J. M. Chow, J. M. Gambetta, L. Frunzioa, S. M. Girvin, M. H. Devoret, and R. J. Schoelkopf, Nature **467**, 574 (2010).
[12] M. Neeley, R. C. Bialczak, M. Lenander, E. Lucero, M. Mariantoni, A. D. O'Connell, D. Sank, H. Wang, M. Weides, J. Wenner, Y. Yin, T. Yamamoto, A. N. Cleland, and J. M. Martinis, Nature **467**, 570 (2010).
[13] B. Röthlisberger, J. Lehmann, D. S. Saraga, P. Traber, and D. Loss, Phys. Rev. Lett. **100**, 100502 (2008).
[14] A. Sharma and P. Hawrylak, Phys. Rev. B **83**, 125311 (2011).
[15] J. Levy, Phys. Rev. Lett. **89**, 147902 (2002).
[16] D. Loss and D. P. DiVincenzo, Phys. Rev. A **57**, 120 (1998).
[17] R. C. Ashoori, Nature (London) **379**, 413 (1996).
[18] S. M. Reimann and M. Manninen, Rev. Mod. Phys. **74**, 1283 (2002).
[19] H. Saarikoski, S. M. Reimann, A. Harju, and M. Manninen, Rev. Mod. Phys. **82**, 2785 (2010).
[20] J. M. Taylor, J. R. Petta, A. C. Johnson, A. Yacoby, C. M. Marcus, and M. D. Lukin, Phys. Rev. B **76**, 035315 (2007).
[21] J. Petta, A. Johnson, J. Taylor, E. Laird, A. Yacoby, M. Lukin, C. Marcus, M. Hanson, and A. Gossard, Science **309**, 2180 (2005).
[22] S. Foletti, H. Bluhm, D. Mahalu, V. Umansky, and A. Yacoby, Nat. Phys. **5**, 903 (2009).
[23] M. Shulman, O. Dial, S. Harvey, H. Bluhm, V. Umansky, and A. Yacoby, Science **336**, 202 (2012).
[24] D. Stepanenko and G. Burkard, Phys. Rev. B **75**, 085324 (2007).
[25] J. Taylor, H. Engel, W. Dür, A. Yacoby, C. Marcus, P. Zoller, and M. Lukin, Nat. Phys. **1**, 177 (2005).
[26] I. van Weperen, B. D. Armstrong, E. A. Laird, J. Medford, C. M. Marcus, M. P. Hanson, and A. C. Gossard, Phys. Rev. Lett. **107**, 030506 (2011).
[27] T. Hiltunen, J. Ritala, T. Siro, and A. Harju, New J. Phys. **15**, 103015 (2013).
[28] E. Nielsen, R. W. Young, R. P. Muller, and M. S. Carroll, Phys. Rev. B **82**, 075319 (2010).
[29] V. Coffman, J. Kundu, and W. K. Wootters, Phys. Rev. A **61**, 052306 (2000).
[30] G. Ramon, Phys. Rev. B **84**, 155329 (2011).
[31] A. V. Khaetskii, D. Loss, and L. Glazman, Phys. Rev. Lett. **88**, 186802 (2002).
[32] F. H. L. Koppens, J. A. Folk, J. M. Elzerman, R. Hanson, L. H. W. van Beveren, I. T. Vink, H. P. Tranitz, W. Wegscheider, L. P. Kouwenhoven, and L. M. K. Vandersypen, Science **309**, 1346 (2005).
[33] O. E. Dial, M. D. Shulman, S. P. Harvey, H. Bluhm, V. Umansky, and A. Yacoby, Phys. Rev. Lett. **110**, 146804 (2013).